JACS
JOURNAL OF THE AMERICAN CHEMICAL SOCIETY
Article
pubs.acs.org/JACS

Structural and Energetic Effects in the Molecular Recognition of Amino Acids by 18-Crown-6

Yu Chen and M. T. Rodgers*

Department of Chemistry, Wayne State University, Detroit, Michigan 48202, United States

Supporting Information

ABSTRACT: Absolute 18-crown-6 (18C6) affinities of five amino acids (AAs) are determined using guided ion beam tandem mass spectrometry techniques. The AAs examined in this work include glycine (Gly), alanine (Ala), lysine (Lys), histidine (His), and arginine (Arg). Theoretical electronic structure calculations are performed to determine stable geometries and energetics for neutral and protonated 18C6 and the AAs as well as the proton bound complexes comprised of these species, $(AA)H^+(18C6)$. The proton affinities (PAs) of Gly and Ala are lower than the PA of 18C6, whereas the PAs of Lys, His, and Arg exceed that of 18C6. Therefore, the collision-induced dissociation (CID) behavior of the $(AA)H^+(18C6)$ complexes differs markedly across these systems. CID of the complexes to Gly and Ala produces $H^+(18C6)$ as the dominant and lowest energy pathway. At elevated energies, $H^+(AA)$ was produced in competition with $H^+(18C6)$ as a result of the relatively favorable entropy change in the formation of $H^+(AA)$. In contrast, CID of the complexes to the protonated basic AAs results in the formation of $H^+(AA)$ as the only direct CID product. $H^+(18C6)$ was not observed, even at elevated energies, as a result of unfavorable enthalpy and entropy change associated with its formation. Excellent agreement between the measured and calculated $(AA)H^+-18C6$ bond dissociation energies (BDEs) is found with M06 theory for all complexes except $(His)H^+(18C6)$, where theory overestimates the strength of binding. In contrast, B3LYP theory significantly underestimates the $(AA)H^+-18C6$ BDEs in all cases. Among the basic AAs, Lys exhibits the highest binding affinity for 18C6, suggesting that the side chains of Lys residues are the preferred binding site for 18C6 complexation in peptides and proteins. Gly and Ala exhibit greater 18C6 binding affinities than Lys, suggesting that the N-terminal amino group provides another favorable binding site for 18C6. Trends in the 18C6 binding affinities among the five AAs examined here exhibit an inverse correlation with the polarizability and proton affinity of the AA. Therefore, the ability of the N-terminal amino group to compete for 18C6 complexation is best for Gly and should become increasing less favorable as the size of the side chain substituent increases.

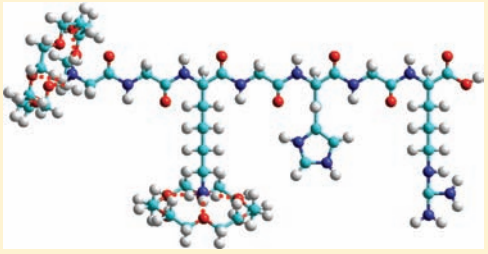

INTRODUCTION

Protein structures and protein−protein interactions play critical roles in biological processes. Binding "hot spots" typically refer to an ∼600 Å^2 region on the surface of a protein at or near the geometric center of the protein−protein interface, and have been identified in a number of protein interfaces.[1−4] These "hot spots" are absolutely essential for protein−protein interactions and contribute significantly to the stability of protein−protein complexes. Therefore, protein structure elucidation and protein surface recognition may provide insight into how proteins interact with each other.

X-ray crystallography[5] and NMR spectroscopy[6,7] are well-established techniques that have been implemented to study protein structures. However, X-ray analyses require sample crystallization, while NMR studies require a large quantity of the protein in a specific solvent. In contrast, mass spectral analyses are not subject to these limitations. Therefore, mass spectrometry (MS) has become an increasingly important tool for protein structure determination due to its speed, sensitivity, and specificity.[8,9]

Hydrogen/deuterium exchange (H/D exchange)[9−16] is an effective mass spectrometric technique based on the solution phase exchange of backbone amide hydrogen atoms with deuterium to explore protein structure. Amide hydrogen atoms on the surface of a protein undergo exchange reactions with deuterium rapidly. In contrast, amide hydrogen atoms that are involved in intramolecular hydrogen bonds exchange very slowly. The exchange rate is primarily determined by solvent accessibility, and whether the amine hydrogen atoms are involved in hydrogen bonding interactions. Therefore, protein structural information can be correlated to the rates of H/D exchange, making H/D exchange a useful technique for studying protein structure and dynamics.

Chemical cross-linking is also a well-established mass spectrometric technique that can be used to study protein three-dimensional structures and protein−protein interactions.[17−26] Cross-linking reactions are carried out using homo- or heterobifunctional cross-linking reagents, binding to specific functional targets, to impose a distance constraint on the respective side chains of proteins. Therefore, protein folding and protein−protein interaction information can be

Received: November 23, 2011
Published: March 8, 2012

dx.doi.org/10.1021/ja211021h | J. Am. Chem. Soc. 2012, 134, 5863−5875

extrapolated based on the length and conformation of the cross-linking reagent.

Selective noncovalent adduct protein probing (SNAPP) has been developed to exploit protein structure and folding states in solution.[27−36] SNAPP relies on the selective binding of a crown ether to basic amino acid (AA) residues, and in particular lysine (Lys) residues, to facilitate rapid identification and characterization of protein sequence, structure, and conformational changes. Therefore, SNAPP can be used to provide information that is key to understanding functional behavior in biological systems at the molecular level. 18-Crown-6 (18C6) is most commonly employed as a protein side chain tag because of its enzyme-like specificity in its interactions with Lys side chains. The extent of 18C6 attachment to a protein is determined by the degree of accessibility to its Lys side chains. When a Lys side chain engages in intramolecular interactions such as a hydrogen bond or salt bridge, the intramolecular interaction generally prevents the attachment of 18C6. Therefore, the number of 18C6 ligands that bind is also directly correlated to the protein structure. Because the number of 18C6 ligands that bind to a protein can be easily determined by MS due to the mass shift, protein structure and folding information under varying solution conditions can be extrapolated. For example, attachment of 18C6 to Calmodulin-Ca^{2+} induces substantial conformational rearrangement as reflected by the number and intensity of 18C6 binding to the protein detected by MS.[33] The number of 18C6 ligands that bind to α-synuclein, a protein associated with the pathology of Parkinson's disease, changes significantly in the presence of Al^{3+}, suggesting that Al^{3+} binding induces dramatic conformational changes. In contrast, the binding of Cu^{2+} does not cause a dramatic change in the 18C6 SNAPP distribution, suggesting that the structural rearrangement induced by the presence of Cu^{2+} is minimal.[33]

The use of molecular recognition of crown ethers by various protein sequences and structures has also been pursued in other groups. Schalley and co-workers[37] applied molecular recognition between 18C6 and oligolysine peptides to investigate molecular mobility, which has attracted considerable attention in supramolecular chemistry and biochemistry. They utilized H/D exchange methods to investigate whether 18C6 moves along an oligolysine scaffold by hopping from one Lys side chain to the other. They reported the observation of highly dynamic motion of 18C6 along oligolysine peptide chains, suggesting that many biologically relevant noncovalently bound complexes may exhibit dynamic behavior that has yet to be recognized. They proposed a mechanism for the dynamic motion of 18C6 along oligolysine peptide chains that proceeds by simultaneous transfer of 18C6 from its ammonium ion binding site to a nearby amino group together with an excess proton. Robinson and co-workers reported a novel charge reduction approach that is based on the collision-induced removal of noncovalently attached aza-18C6 from the charged side chain of tetrameric human transthyretin (TTR).[38] The selective binding of the crown ether to the protein contributes to the low quantity of aza-18C6 required, and leads to a reduced chance of unintended side reactions in solution. Reduction of the charge state using molecular recognition of aza-18C6 does not cause dramatic structural change. Therefore, it significantly improves the stability of protein complexes, and protects the native state of proteins. Brodbelt and co-workers reported a method using a chromophore, an 18C6 derivative, to study fragmentation patterns of peptides.[39] In their study, the chromophore was noncovalently attached to a Lys side chain via three hydrogen bonds. The chromophore facilitates peptides fragmentation by absorbing UV irradiation and transferring it to the peptide by intramolecular vibrational redistribution (IVR) in the gas phase. Oshima and co-workers applied dicyclohexano−18C6 (DCH18C6) as an affinity ligand to extract the lysine-rich protein, cytochrome *c*, in the Li_2SO_4/polyethylene glycol (PEG) aqueous two-phase system.[40] With this technique, cytochrome *c* can be quantitatively extracted into the PEG-rich phase in the presence of DCH18C6 within 5 min.

The charged AAs, Lys, histidine (His), arginine (Arg), glutamic acid (Glu), and aspartic acid (Asp) offer the best targets for molecular recognition of specific side chains in peptides or proteins. As a result of the structural similarity of the acidic AAs, Glu and Asp, which differ only in number of methylene groups in the side chain, these acidic AAs are difficult to distinguish. The basic AAs, Lys, His, and Arg offer the possibility of achieving specificity due to the different chemical functionalities of the basic side chains. Glycine (Gly) and alanine (Ala) are good models for molecular recognition of the N-terminus in peptides and proteins because the N-terminal amino group is the only favorable binding site for 18C6 complexation to these two AAs.

Julian and co-workers applied a site-directed mutagenesis approach, in which Lys residues of a series of ubiquitin mutants were exchanged for asparagine one at a time, to investigate the mechanism of the SNAPP method.[34] They found that Lys reactivity follows the order, noninteracting Lys > Lys involved in hydrogen bonding interactions > Lys participating in salt bridges. Surface availability does not ensure the attachment of 18C6. However, lack of surface accessibility will constrain the attachment of 18C6. Interestingly, they observed SNAPP distributions with complexation of up to six 18C6 ligands although the number of Lys residues was only five in the ubiquitin mutant, indicating that some residues other than Lys may also contribute to the SNAPP distribution. Coincidently, our previous study of protonated peptidomimetic base−18C6 complexes found that the N-terminal amino group mimic, *i*-propylamine (IPA), exhibits a higher 18C6 binding affinity than that of the Lys mimic, *n*-butylamine (NBA).[41] This result indicates that binding to the N-terminal amino group may also contribute to the SNAPP distribution, and may provide an explanation for their results.

Accurate structural and thermochemical information regarding the binding between 18C6 and the AAs may provide insight into the selectivity of the complexation process. However, very limited thermochemical data has thus far been reported in the literature. In previous work, we examined the interactions between a series of protonated peptidomimetic bases that serve as mimics of the N-terminal amino group and the side chains of the basic AAs in peptides and proteins. The protonated peptidomimetic bases investigated in that work include IPA as a mimic for the N-terminal amino group, NBA as well as a series of other primary amines as mimics for the side chain of Lys, imidazole and 4-methylimidazole as mimics for the side chain of His, and 1-methylguanidine as a mimic for the side chain of Arg. Using energy-resolved collision-induced dissociation (CID) techniques and theoretical electronic structure calculations, we reported structures and 18C6 binding affinities for the complexes investigated. The measured 18C6 binding affinities follow the order: IPA > NBA > IMID > MGD > 4MeIMID, suggesting that binding to the N-terminal amino

group is most favorable followed by Lys residues. The relative binding affinities of the His and Arg side chain mimics make it unclear as to which AA, His or Arg, will bind 18C6 most effectively.

In the present study, we extend this work to explicitly include five AAs. Again using both guided ion beam tandem mass spectrometry techniques and theoretical electronic structure calculations. We characterize the structures of protonated amino acid−18C6 complexes and measure the absolute 18C6 binding affinities of the protonated AAs to provide further insight into the molecular recognition of AAs, and by inference, peptides and proteins by 18C6. The AAs examined in the present study include Gly, Ala, Lys, His, and Arg as shown schematically in the model peptide of Figure 1. The energy-

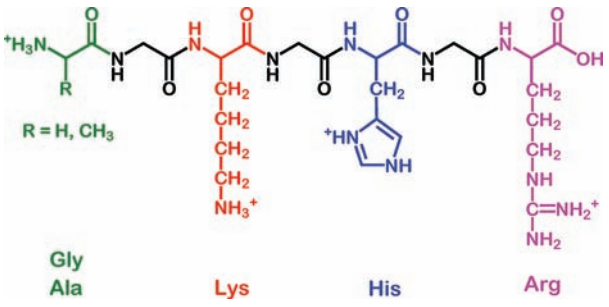

Figure 1. Model peptide showing the structures of the amino acids examined here including: Gly, Ala, Lys, His, and Arg.

dependent cross sections for CID are analyzed using methods previously developed that explicitly include the effects of the kinetic and internal energy distributions of the reactants, multiple ion-neutral collisions, and the kinetics of unimolecular dissociation. Absolute $(AA)H^+$−18C6 bond dissociation energies (BDEs) for five $(AA)H^+(18C6)$ complexes are derived and compared to theoretical estimates determined using M06 and B3LYP theory. Absolute $(18C6)H^+$−AA BDEs are also determined for the complexes to Gly and Ala and compared with theory.

EXPERIMENTAL SECTION

General Procedures. Cross sections for CID of five protonated amino acid−18C6 complexes, $(AA)H^+(18C6)$ with Xe, where AA = Gly, Ala, Lys, His, and Arg, are measured using a guided ion beam tandem mass spectrometer that has been described in detail previously.[42] The $(AA)H^+(18C6)$ complexes are generated by electrospray ionization (ESI)[41,43] using a home-built source similar in design to that developed by Moison et al.[43] Droplets emanating from the 35 gauge SS ESI needle are introduced into the vacuum region through capillary tubing, biased at 20−50 V, and heated to 90−130 °C. Ions are focused by an rf ion funnel, similar in design to that developed by Smith and co-workers.[44,45] The ion funnel facilitates efficient transfer of ions from the high pressure source region to the low pressure region of the mass spectrometer. A linear dc gradient is applied across the ion funnel by applying a dc voltage to the first and last plates of the ion funnel with a resistor chain connecting all intervening plates. Adjacent electrodes receive equal and opposite phases of an rf signal with peak-to-peak voltage in the range between 10 and 30 V, and is operated at a frequency in the range between 0.6 and 1.2 MHz. This oscillating field on the plates focuses ions radially to the center of the ion funnel. Ions emanating from the ion funnel are thermalized in the hexapole ion guide by collisions with the background gases. The ions are effusively sampled from the ESI source region, focused, accelerated, and focused into a magnetic sector momentum analyzer for mass analysis. Mass-selected ions are decelerated to a desired kinetic energy and focused into an octopole ion guide. The octopole passes through a static gas cell containing Xe at low pressure (~0.05−0.20 mTorr) to ensure that multiple ion-neutral collisions are improbable. The octopole acts as an efficient trap for ions in radial direction.[46] Therefore, loss of scattered reactant and product ions in the octopole region is almost entirely eliminated. Xe is used as the collision gas because it is heavy and polarizable, and therefore leads to more efficient kinetic to internal energy transfer in the CID process.[47,48] Products and unreacted beam ions drift to the end of the octopole, are focused into a quadrupole mass filter for mass analysis, and are subsequently detected with a secondary electron scintillation detector and standard pulse counting techniques.

Data Handling. Ion intensities are converted to absolute cross sections using a Beer's law analysis as described previously.[49] Errors in the pressure measurement and uncertainties in the length of interaction region lead to ±20% uncertainties in the cross-section magnitudes. Relative uncertainties are approximately ±5%.

Ion kinetic energies in the laboratory frame, E_{lab}, are converted to energies in the center-of-mass frame, E_{CM}, using the formula $E_{CM} = E_{lab}m/(m + M)$, where M and m are the masses of the ionic and neutral reactants, respectively. All energies reported below are in the center-of-mass frame unless otherwise noted. The absolute zero and distribution of the ion kinetic energies are determined using an octopole ion guide as a retarding potential analyzer as previously described.[49] The distribution of ion kinetic energies is nearly Gaussian with a full width at half-maximum (fwhm) between 0.2 and 0.5 eV (lab) for these experiments. The uncertainty in the absolute energy scale is ±0.05 eV (lab).

Because multiple ion-neutral collisions can influence the shape of CID cross sections, particularly in the threshold region, the CID cross section for each complex was measured twice at three nominal pressures (0.05, 0.1, 0.2 mTorr). Data free from pressure effects are obtained by extrapolating to zero pressure of the Xe reactant, as described previously.[50] Therefore, the zero-pressure extrapolated cross sections subjected to thermochemical analysis are the result of single $(AA)H^+(18C6)$−Xe collisions.

Theoretical Calculations. To obtain stable geometries, vibrational frequencies, and energetics for neutral and protonated 18C6 and the AAs, as well as the proton bound $(AA)H^+(18C6)$ complexes, theoretical calculations were performed using HyperChem[51] and the Gaussian 09[52] suite of programs. Neutral and protonated 18C6 and the AAs exhibit many stable low-energy structures. Therefore, potential low-energy candidate structures were obtained via a 300 cycle simulated annealing procedure employing the Amber force field. A three phase annealing process was used, with each cycle beginning and ending at 0 K, lasting for 0.8 ps, and achieving a simulation temperature of 1000 K. Heating and cooling times for each cycle were 0.3 ps each, allowing 0.2 ps for the ions to sample conformational space at the simulation temperature. Relative energies were computed using molecular mechanics methods every 0.001 ps. The most stable conformers accessed at the end of each annealing cycle were subjected to additional analysis. All structures within 30 kJ/mol of the lowest-energy structure found via the simulated annealing procedure, as well as others representative and encompassing the entire range of structures found, were further optimized using density function theory.

Geometry optimizations for neutral and protonated 18C6 and the AAs as well as the proton bound $(AA)H^+(18C6)$ complexes were performed using density functional theory at the B3LYP/6-31G* level.[53,54] Vibrational analyses of the geometry-optimized structures were performed to determine the vibrational frequencies of the optimized species for use in modeling of the CID data. The frequencies calculated were scaled by a factor of 0.9804.[55] The scaled vibrational frequencies and rotational constants are listed in Tables S1 and S2 of the Supporting Information. Single-point energy calculations were performed at the B3LYP/6-311+G(2d,2p) and M06/6-311+G-(2d,2p) levels of theory using the B3LYP/6-31G* optimized geometries. To obtain accurate energetics, zero-point energy (ZPE) and basis set super position error (BSSE) corrections are included in the computed BDEs using the counterpoise approach.[56,57]

dx.doi.org/10.1021/ja211021h | J. Am. Chem. Soc. 2012, 134, 5863−5875

Polarizability is one of the key factors that contribute to the strength of noncovalent interactions. Thus, the isotropic molecular polarizabilities of the ground-state conformations of the neutral and protonated AAs are calculated based on PBE0 hybrid functional and the 6-311+G(2d,2p) basis set using the B3LYP/6-31G* optimized geometries. This level of theory was chosen because polarizabilities determined using the PBE0 functional[58] exhibit very good agreement with experimentally determined polarizabilities.[59]

Thermochemical Analysis. The threshold regions of the CID cross sections were modeled using an empirical threshold energy law, eq 1

$$\sigma(E) = \sigma_0 \sum_i g_i (E + E_i - E_0)^n / E \quad (1)$$

where σ_0 is an energy independent scaling factor, E is the relative translational energy of the reactants, E_0 is the threshold for reaction of the ground electronic and ro-vibrational state, and n is an adjustable parameter that describes the efficiency of kinetic to internal energy transfer.[60] The summation is over the ro-vibrational states of the reactant (AA)H$^+$(18C6) complexes, i, where E_i is the excitation energy of each state and g_i is the population of that state ($\sum g_i = 1$). The relative reactivity of all ro-vibrational states, as reflected by σ_0 and n, is assumed to be equivalent.

CID of the (Gly)H$^+$(18C6) and (Ala)H$^+$(18C6) complexes results in two reactions occurring in parallel and competing with each other. To examine the effects of competition on the measured CID cross sections and extract accurate threshold values from the experimental data, the modified model of eq 2 based on eq 1 was used to simultaneously analyze the thresholds for these systems.

$$\sigma_j(E) = \frac{n\sigma_{0,j}}{E} \sum_i g_i \int_0^{E+E_i-E_0} \frac{k_j(E^*)}{k_{tot}(E^*)} [1 - e^{-k_{tot}(E*)\tau}] \times (\Delta E)^{n-1} d(\Delta E) \quad (2)$$

The indices j refer to a particular product channel, $k_{tot} = \sum k_j$, and all rate constants are calculated using Rice–Ramsperger–Kassel–Marcus (RRKM) theory. The ratio of dissociation rates k_j/k_{tot} introduces the coupling between product channels j. The scaling factors $\sigma_{0,j}$ are ideally the same for all product channels; however, independent scaling is needed to accurately reproduce the cross-section magnitudes in these systems. E^* is the internal energy of the energized molecule after collision, $E^* = E + E_i - \Delta E$, where E and E_i are as defined in eq 1 and ΔE is the energy that remains in translation after collision between the (AA)H$^+$(18C6) complex and Xe.

The density of ro-vibrations states, i, is determined using the Beyer–Swinehart algorithm,[61−63] and the relative populations, g_i, are calculated for a Maxwell–Boltzmann distribution at 298 K, the internal temperature of the reactants. Vibrational frequencies and rotational constants of the reactant (AA)H$^+$(18C6) complexes are determined as described in the Theoretical Calculations section. The average internal energy at 298 K of the (AA)H$^+$(18C6) complexes and their primary CID products, H$^+$(AA) and 18C6 for all systems, and AA and H$^+$(18C6) for the complexes to Gly and Ala, are included in Table S1 of the Supporting Information. The calculated frequencies are scaled by ±10% to estimate the sensitivity of our analysis to the deviations from the true frequencies as suggested by Pople.[64,65] The corresponding change in the average vibrational energy is assumed to provide a good estimate of one standard deviation of the uncertainty in the vibrational energy (Table S1).

All CID reactions that occur faster than the experimental time scale, ~10^{-4} s, should be observed. However, as the size of the reactant (AA)H$^+$(18C6) complexes increases, there is an increased probability that the CID reaction will not take place within the experimental time scale. Once the lifetime of the energized molecule (EM) approaches this limit, the CID threshold shifts to higher energies, resulting in a kinetic shift. Therefore, statistical theories for unimolecular dissociation were included in the analysis, specifically Rice–Ramsperger–Kassel–Marcus (RRKM) theory, as described in detail elsewhere[66,67] to quantify and correct for the kinetic shift. This requires sets of ro-vibrational frequencies appropriate for the EM and the transition states (TSs) leading to dissociation. The TSs are expected to be loose and product-like and thus are modeled using the ro-vibrational frequencies of the products for these systems. This treatment corresponds to a phase space limit (PSL) in which the TS occurs at the centrifugal barrier for dissociation as described in detail elsewhere.[66] The ro-vibrational frequencies of the EMs and TSs of the (AA)H$^+$(18C6) complexes are given in Tables S1 and S2 of the Supporting Information.

The models represented by eqs 1 and 2 are expected to be appropriate for translationally driven reactions[68] and have been found to reproduce cross sections well in numerous previous studies of CID processes.[69−80] The model is convoluted with the kinetic and internal energy distributions of the reactants, and a nonlinear least-squares analysis of the data is performed to give optimized values for the parameters σ_0, E_0, and n. The errors associated with the measurement of E_0 are estimated from the range of threshold values determined for the zero-pressure-extrapolated data sets for each complex, variations associated with uncertainties in the vibrational frequencies, and the error in the absolute energy scale, ±0.05 eV (lab). For analyses that include the RRKM lifetime analysis, the uncertainties in the reported E_0(PSL) values also include the effects of increasing and decreasing the time assumed available for dissociation (~10^{-4} s) by a factor of 2.

Equations 1 and 2 explicitly include the internal energy of the reactant (AA)H$^+$(18C6) complex, E_i. All energy available is treated statistically because the ro-vibrational energy of the reactants is redistributed throughout the (AA)H$^+$(18C6) complex upon interaction with Xe. Because the CID processes examined here are simple noncovalent bond cleavage reactions, the E_0(PSL) values determined from analysis with eqs 1 and 2 can be equated to 0 K BDEs.[81,82] The accuracy of the thermochemistry obtained by this modeling procedure has been verified for many systems by comparing values derived from other experimental techniques and to ab initio calculations. Absolute BDEs in the range from ~10 to 400 kJ/mol have been accurately determined using threshold collision-induced dissociation (TCID) techniques.[83]

RESULTS

Cross Sections for Collision-Induced Dissociation. Experimental cross sections were obtained for the interaction of Xe with five (AA)H$^+$(18C6) complexes, where AA = Gly, Ala, Lys, His, and Arg. Figure 2 shows representative data for the (Lys)H$^+$(18C6) complex. Experimental cross sections for the other (AA)H$^+$(18C6) complexes are shown in Figure S1 of the Supporting Information. Loss of the intact 18C6 ligand is

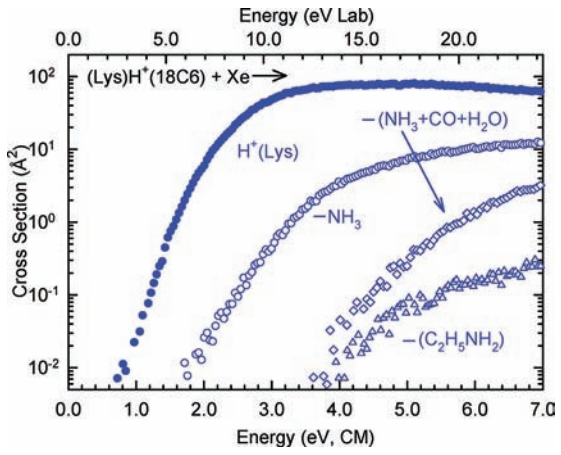

Figure 2. Cross sections for collision-induced dissociation of the (Lys)H$^+$(18C6) complex with Xe as a function of kinetic energy in the center-of-mass frame (lower x-axis) and laboratory frame (upper x-axis). Data are shown for a Xe pressure of 0.2 mTorr.

dx.doi.org/10.1021/ja211021h | J. Am. Chem. Soc. 2012, 134, 5863−5875

observed for all five complexes, CID reactions represented by eq 3,

$$(AA)H^+(18C6) + Xe \rightarrow H^+(AA) + 18C6 + Xe \quad (3)$$

and corresponds to the most favorable process for the complexes to Lys, His, and Arg. The apparent threshold for the $H^+(AA)$ product decreases in the order Gly > Ala > Lys > His > Arg, suggesting that the binding of 18C6 follows that same order. The magnitude of the $H^+(AA)$ cross section increases in nearly the reverse order, Gly < Ala < Arg < His < Lys.

For the complexes to Gly and Ala, loss of the intact AA is observed in competition with loss of 18C6, and corresponds to the lowest-energy CID pathway for these complexes, CID reactions represented by eq 4.

$$(AA)H^+(18C6) + Xe \rightarrow H^+(18C6) + AA + Xe \quad (4)$$

The apparent threshold for the $H^+(18C6)$ product increases from Gly to Ala, whereas the difference in the apparent threshold for $H^+(AA)$ and $H^+(18C6)$ decreases from Gly to Ala, indicating that Ala competes more effectively than Gly for the proton. Thus, the magnitude of the $H^+(AA)$ product cross section is greater for the complex to Ala. At elevated energies, products corresponding to the sequential dissociation of $H^+(18C6)$ were also observed in the complexes to Gly and Ala, reactions represented by eq 5.

$$H^+(18C6) \rightarrow H^+(C_2H_4O)_n + (6 - n)C_2H_4O$$
$$n = 1 - 4 \quad (5)$$

At elevated energies, products corresponding to sequential dissociation of $H^+(AA)$ were also observed for the complexes to Lys, His, and Arg. Sequential dissociation of $H^+(Lys)$ results in the loss of NH_3 and sequential concomitant loss of CO and H_2O from this primary product. At elevated energies, direct loss of ethylamine is also observed.[84,85] Sequential dissociation of $H^+(His)$ results in the loss of $COOH_2$ and sequential loss of NH_3.[84] Sequential dissociation of $H^+(Arg)$ results in the loss of NH_3, loss of guanidine (GD) or protonated guanidine, $H^+(GD)$, as well as the simultaneous loss of NH_3, CO, H_2O, and CN_2H_2.[85] These results are consistent with CID results for the $H^+(Lys)$, $H^+(His)$, and $H^+(Arg)$ complexes previously reported by Siu, Hopkinson, and co-workers.[85] Ligand exchange to produce $XeH^+(AA)$ is only observed for the complex to Arg at elevated energies.

Theoretical Results. Theoretical structures for the neutral and protonated AAs and 18C6 as well as the $(AA)H^+(18C6)$ complexes were calculated as described in the Theoretical Calculations section. The ground-state structures of the $(AA)H^+(18C6)$ complexes are shown in Figure 3. Structures of several representative low-energy conformations of the $(AA)H^+(18C6)$ complexes are shown in Figure S2 of the Supporting Information. Results for the stable low-energy conformations of the neutral and protonated AAs and 18C6 are shown in Figure S3 of the Supporting Information. The conformations of neutral and protonated 18C6 were reported in our previous study; thus, only a few representative structures are provided in the Supporting Information.[41] The $(AA)H^+$–18C6 BDEs at 0 K calculated at the M06/6-311+G(2d,2p)//B3LYP/6-31G* and B3LYP/6-311+G(2d,2p)//B3LYP/6-31G* levels of theory including ZPE and BSSE corrections, are listed in Table 1. Comparison of the measured and calculated values suggests that the M06 results are most reliable.

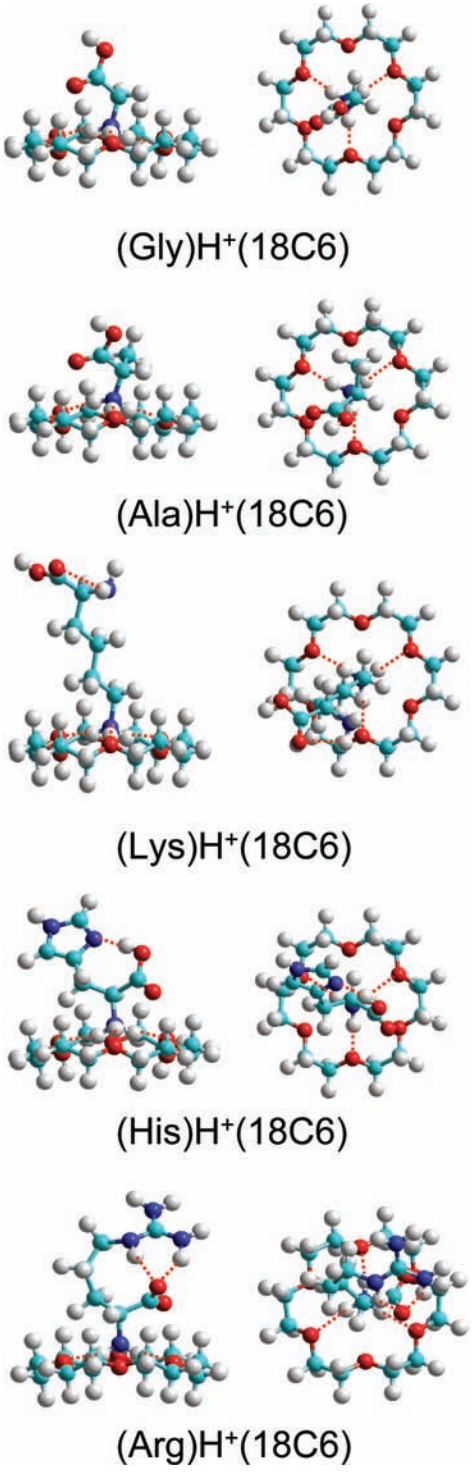

Figure 3. B3LYP/6-31G* optimized geometries of the ground-state conformers of the $(AA)H^+(18C6)$ complexes.

Therefore, the following discussion will focus on the relative energies calculated at the M06/6-311+G(2d,2p) level of theory using the B3LYP/6-31G* optimized structures unless otherwise specified.

Amino Acids. Details of the optimized geometries for the ground-state and stable low-energy conformations of the neutral and protonated AAs are provided in Figure S3 of the Supporting Information. The preferred site of protonation for Gly and Ala is to the N-terminal amino group along the

dx.doi.org/10.1021/ja211021h | J. Am. Chem. Soc. 2012, 134, 5863–5875

Table 1. (AA)H$^+$(18C6) Bond Dissociation Enthalpies at 0 K in kJ/mol[a]

			M06[b]			B3LYP[c]		
AA	ionic product	TCID	D_e	D_0[d]	$D_{0,BSSE}$[d,e]	D_e	D_0[d]	$D_{0,BSSE}$[d,e]
Gly	H$^+$(18C6)	222.9 (10.6)[f]	232.8	217.5	209.3	203.8	188.5	180.9
	H$^+$(Gly)	262.4 (10.6)[f]	285.6	274.8	262.5	242.6	231.7	221.4
Ala	H$^+$(18C6)	216.5 (8.7)[f]	239.4	223.2	214.4	201.6	185.2	177.0
	H$^+$(Ala)	255.0 (9.8)[f]	276.9	264.4	251.4	223.8	211.3	200.5
Lys	H$^+$(Lys)	167.7 (7.1)	190.1	184.3	172.8	152.2	146.5	137.0
His	H$^+$(His)	156.3 (4.6)	208.5	196.4	183.3	157.2	145.1	133.9
Arg	H$^+$(Arg)	141.1 (4.0)	171.3	157.3	143.7	119.6	105.6	93.7
AEU/MAD		7.2 (3.0)[g]		18.9 (12.2)[g]	7.7 (10.9)[g]		28.5 (12.6)[g]	39.2 (12.8)[g]
		9.6 (1.3)[h]		6.0 (0.9)[h]	7.9 (8.1)[h]		32.8 (2.2)[h]	40.8 (1.8)[h]

[a]Present results, uncertainties are listed in parentheses. [b]Calculated at M06/6-311+G(2d,2p)//B3LYP/6-31G* level of theory. [c]Calculated at B3LYP/6-311+G(2d,2p)//B3LYP/6-31G* level of theory. [d]Including ZPE corrections with frequencies scaled 0.9804. [e]Also includes basis BSSE corrections. [f]TCID bond dissociation enthalpies obtained from competitive analyses. [g]Values for (AA)H$^+$−18C6. [h]Values for (18C6)H$^+$−AA.

backbone. In contrast, protonation of the side chain substituent is preferred for the basic AAs, Lys, His, and Arg.

The ground-state and several stable low-energy conformers of Gly and H$^+$(Gly) are shown in the Supporting Information, Figure S3. In the ground-state structure of neutral Gly, the N-terminal amino group points away from the CH_2 group, consistent with the structure found by Cassady and co-workers.[86] The ground-state structure of Ala exhibits a similar conformation to that of Gly. In the ground-state structure of H$^+$(Gly), one of the N-terminal amino hydrogen atoms points toward the carbonyl oxygen atom forming an intramolecular hydrogen bond. However, geometry optimization of the ground-state structure found by Cassady and co-workers using HF/6-31G* theory[86] corresponds to a transition state structure, as shown in Figure S3 of the Supporting Information. The ground-state structure of H$^+$(Gly) found in the present study was also reported by Armentrout and co-workers.[87] The ground-state structure of H$^+$(Ala) exhibits a similar conformation with the backbone hydrogen atom substituted by a methyl group.

The ground-state and several stable low-energy conformers of Lys and H$^+$(Lys) are shown in the Supporting Information, Figure S3. The ground-state structures of Lys and H$^+$(Lys) found in the present study are consistent with the structures reported by Williams and co-workers.[88] The ground-state structure of Lys is stabilized by two intramolecular hydrogen bonds, one between the amino nitrogen atom of the side chain and the backbone hydroxyl hydrogen atom, and the other between the carbonyl oxygen atom and one of the amino hydrogen atoms of the backbone. The ground-state structure of H$^+$(Lys) is also stabilized by two intramolecular hydrogen bonds. The protonated amino group of the side chain forms two intramolecular hydrogen bonds with the backbone amino nitrogen and carbonyl oxygen atoms.

The ground-state and several stable low-energy conformers of His and H$^+$(His) are shown in the Supporting Information, Figure S3. The ground-state structure of His is stabilized by two intramolecular hydrogen bonds between the imine hydrogen and the carbonyl oxygen atoms and between the hydroxyl hydrogen and the backbone amino nitrogen atom, consistent with the structure found by Dunbar, Siu, and co-workers.[89] The ground-state structure of H$^+$(His) is also stabilized by two intramolecular hydrogen bonds, one between the protonated side chain amino hydrogen and backbone amino nitrogen atoms, and the other between the backbone amino hydrogen and carbonyl oxygen atoms. The ground-state structure found in the present work was also reported by Kovacevic and co-workers.[90] The ground-state structure reported by Amster and co-workers involves a hydrogen bond between the protonated side chain and the carbonyl oxygen atom.[91] However, present calculations suggest that this conformer lies 4.8 kJ/mol higher in energy than the ground-state conformer determined here.

The ground-state and several stable low-energy conformers of Arg and H$^+$(Arg) are shown in the Supporting Information, Figure S3. The ground-state structures of neutral and protonated Arg determined here are consistent with structures previously reported by Gutowski, Williams, and Jockusch.[92,93] The ground-state structure of Arg is stabilized by three intramolecular hydrogen bonds, one between the backbone amino nitrogen and the hydroxyl hydrogen atoms, one between one of the primary amine hydrogen atoms of side chain and the backbone carboxyl oxygen atom, and the third between one of the primary amine hydrogen atoms of backbone and the imine nitrogen atom of side chain.[92] In the ground-state conformer of H$^+$(Arg), the protonated side chain forms two intramolecular hydrogen bonds with the backbone amino nitrogen and the carbonyl oxygen atoms.[93]

18C6. The present work is a follow-up to an earlier study, where we examined the interactions between a series of protonated peptidomimetic bases and 18C6.[41] Because the neutral and protonated forms of 18C6 were examined in detail in that work, only a brief summary of the theoretical results are discussed here and shown in Figure S3 of the Supporting Information. The ground-state conformation of neutral 18C6 is of C_i symmetry; four of its six ether oxygen atoms are directed inward from the ether backbone, while the other two are directed outward. A weak intramolecular C−H···O interaction helps stabilize the ground-state conformer. A stable conformer with D_{3d} symmetry was also found that lies 9.3 kJ/mol higher in energy than the ground-state structure. In this conformation, each of the oxygen atoms are directed inward from the ether backbone, forming a nucleophilic cavity for very favorable interaction with guest cations.

In the ground-state conformation of H$^+$(18C6), the proton binds to an O atom and is stabilized by an O1···H$^+$···O3 hydrogen bond. The ground-state of H$^+$(18C6) exhibits a boat-like conformation where the crown folds up to better solvate the excess proton. A relatively flat conformation of H$^+$(18C6) where the proton is again stabilized between the O1 and O3

dx.doi.org/10.1021/ja211021h | J. Am. Chem. Soc. 2012, 134, 5863−5875

Table 2. Fitting Parameters of Eqs 1 and 2, Threshold Dissociation Energies at 0 K, and Entropies of Activation at 1000 K of (AA)H$^+$(18C6) Complexes[a]

AA	ionic product	σ_o[b]	n[b]	E_0[c] (eV)	E_0 (PSL)[b] (eV)	kinetic shift (eV)	$\Delta S^{\ddagger}$(PSL) (J mol^{-1} K^{-1})
Gly[d]	H$^+$(18C6)	28.5 (7.4)	0.8 (0.1)	4.10 (0.14)	2.13 (0.11)	1.97	86 (4)
	H$^+$(Gly)	7.0 (1.4)	1.5 (0.1)	4.54 (0.07)	2.37 (0.10)	2.17	101 (4)
Gly[e]	H$^+$(18C6)	37 (11)	0.6 (0.1)	-	2.32 (0.11)	-	85 (4)
	H$^+$(Gly)	0.9 (0.2)	0.6 (0.1)	-	2.72 (0.12)	-	113 (4)
Ala[d]	H$^+$(18C6)	10.8 (2.6)	1.2 (0.2)	3.74 (0.11)	2.04 (0.09)	1.70	105 (4)
	H$^+$(Ala)	14.8 (2.7)	1.2 (0.1)	4.59 (0.08)	2.43 (0.09)	2.16	130 (4)
Ala[e]	H$^+$(18C6)	1.2 (0.3)	0.5 (0.1)	-	2.24 (0.10)	-	105 (4)
	H$^+$(Ala)	16.7 (5.6)	0.5 (0.1)	-	2.64 (0.10)	-	129 (4)
Lys	H$^+$(Lys)[f]	108 (12)	0.8 (0.1)	3.79 (0.09)	1.98 (0.07)	1.81	122 (4)
	H$^+$(Lys)[g]	122 (12)	0.7 (0.1)	3.83 (0.09)	1.74 (0.07)	2.09	61 (4)
His	H$^+$(His)[f]	15.7 (1.2)	1.7 (0.1)	2.68 (0.09)	1.62 (0.05)	1.06	128 (4)
	H$^+$(His)[g]	16.3 (1.5)	1.7 (0.1)	2.69 (0.09)	1.61 (0.05)	1.08	114 (4)
Arg	H$^+$(Arg)[f]	10.1 (0.9)	1.6 (0.1)	2.37 (0.09)	1.46 (0.04)	0.91	138 (4)
	H$^+$(Arg)[g]	9.9 (1.0)	1.6 (0.1)	2.37 (0.09)	1.36 (0.05)	1.01	101 (4)

[a]Present results, uncertainties are listed in parentheses. [b]Average values for loose PSL transition state. [c]No RRKM analysis. [d]Values obtained for independent fits to the CID product channels. [e]Values obtained for competitive fits to the CID product channels. [f]Values obtained for fits using parameters derived from the most stable backbone binding conformation. [g]Values obtained for fits using parameters derived from the most stable side chain binding conformation.

oxygen atoms was also found that lies 31.1 kJ/mol higher in energy than the ground-state structure.

(AA)H$^+$(18C6) Complexes. The ground-state conformations of the (AA)H$^+$(18C6) complexes are shown in Figure 3, while select excited low-energy conformers are shown in Figure S2 of the Supporting Information. 18C6 binds to the protonated backbone amino group in the complexes to Gly, Ala, Arg, and His, whereas binding to the protonated side chain substituent is preferred for the complex to Lys. In all cases, binding occurs via three nearly ideal N−H···O hydrogen bonds. The conformation of 18C6 in all of these complexes bears great similarity to the D_{3d} excited conformer of the neutral crown with a nucleophilic cavity in the center for interaction with the protonated AA.

In the ground-state conformations of the (Gly)H$^+$(18C6) and (Ala)H$^+$(18C6) complexes, the conformations of H$^+$(Gly) and H$^+$(Ala) are remarkably similar to the conformations of the isolated ground-state species. In both cases, the protonated backbone amino group interacts with 18C6 via three nearly ideal N−H···O hydrogen bonds. In the ground-state conformation of the (Lys)H$^+$(18C6) complex, the H$^+$(Lys) moiety is stabilized by an intramolecular hydrogen bond between a backbone amino hydrogen and carbonyl oxygen atoms. The H$^+$(Lys) moiety exhibits an extended conformation, resulting in the protonated amino group of the side chain interacting with 18C6 via three nearly ideal N−H···O hydrogen bonds. Several excited conformers where 18C6 also interacts with the protonated amino group of the side chain, but that differ in the conformation of the AA backbone were also found; an example is shown in Figure S2 of the Supporting Information. Likewise, excited conformers with 18C6 bindings to the protonated backbone amino group were also found, but the most stable of these conformers is 4.2 kJ/mol less stable than the ground-state conformer determined here. Thus, binding to the side chain of Lys is favored over binding to the backbone by at least 4.2 kJ/mol. Attempts to calculate salt bridge structures in which 18C6 binds to the either the protonated side chain or the protonated backbone always converged to one of the low-energy nonsalt bridge structures shown in Figure S2 except when open structures with no hydrogen bond stabilization between the protonated amino and carboxylate groups are computed. However, such zwitterionic complexes are at least 179 kJ/mol less stable than the ground-state conformer.

In the ground-state conformation of the (His)H$^+$(18C6) complex, the proton binds to the backbone amino group of His to form H$^+$(His), which binds to a distorted D_{3d} conformer of 18C6 via three nearly ideal N−H···O hydrogen bonds. The conformation of the H$^+$(His) moiety in this complex is stabilized by an intramolecular hydrogen bond between the backbone carboxyl hydrogen and side chain imine nitrogen atoms. Stable conformations are also found where the proton binds to the protonated side chain of His and the H$^+$(His) moiety binds to 18C6 via two N−H···O hydrogen bonds as shown in Figure S2 of the Supporting Information. However, these conformers are calculated to be at least 36.9 kJ/mol less stable than the ground-state conformer. Again attempts to calculate salt bridge structures (where both the backbone amino group and side chain are protonated and the carboxyl group is deprotonated) in which 18C6 binds to the protonated backbone amino group always converged to the ground-state conformation. Attempts to calculate salt bridge structures in which 18C6 binds to the either the protonated side chain or the protonated backbone always converged to one of the low-energy nonsalt bridge structures shown in Figure S2.

The ground-state conformation of the (Arg)H$^+$(18C6) complex is a salt bridge structure in which both the backbone amino group and side chain are protonated, while the carboxyl group is deprotonated, and the protonated backbone amino group of the H$^+$(Arg) moiety binds to a distorted D_{3d} conformer of 18C6 via three nearly ideal N−H···O hydrogen bonds. The H$^+$(Arg) moiety is stabilized by two intramolecular hydrogen bonds between the amine and imine hydrogen atoms of the protonated side chain and one of the backbone carboxylate oxygen atoms. Stable conformations are also found where only the side chain is protonated, and the protonated side chain of the H$^+$(Arg) moiety binds to 18C6 via three N−H···O hydrogen bonds to the O1, O2, and O4 atoms of 18C6 as shown in Figure S2 of the Supporting Information. However, the most stable conformer of this nature is calculated to be 13.9 kJ/mol less stable than the ground-state conformer.

dx.doi.org/10.1021/ja211021h | J. Am. Chem. Soc. 2012, 134, 5863−5875

Stable conformations are also found where only the backbone is protonated, and the protonated backbone amino group of the H^+(Arg) moiety binds via three nearly ideal N−H···O hydrogen bonds. However, the most stable conformer of this nature is calculated to be 42.7 kJ/mol less stable than the ground-state conformer. Other salt bridge conformations involving 18C6 binding to the protonated side chain were also investigated. However, these structures always converged to nonsalt bridge conformations.

Threshold Analysis. The model of eq 1 was used to analyze the thresholds for reactions 3 in five (AA)H^+(18C6) complexes, where AA = Gly, Ala, Lys, His, and Arg. The results of these analyses are provided in Table 2 and representative results are shown in Figure 4 for the (Lys)H^+(18C6) complex.

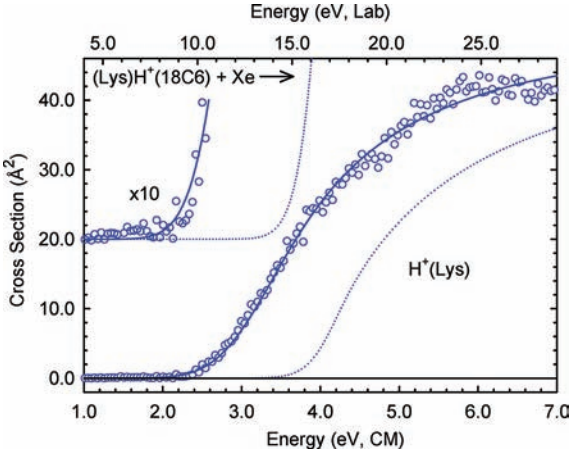

Figure 4. Zero-pressure-extrapolated H^+(Lys) CID product cross section of the (Lys)H^+(18C6) complex in the threshold region. The solid lines show the best fits to the data using eq 1 convoluted over the ion and neutral kinetic energy distributions. The dotted lines show the model cross sections in the absence of experimental kinetic energy broadening for reactants with an internal energy corresponding to 0 K.

The analyses for the other (AA)H^+(18C6) complexes are shown in Figure S4 of the Supporting Information. For the complexes to Lys, His, and Arg, the data were analyzed in two ways. First, the CID cross sections were analyzed assuming that the most stable backbone binding conformations of the (AA)H^+(18C6) complexes were accessed in the experiments, that is, the ground-state conformations of the complexes to His and Arg, and an excited conformation of the complex to Lys. Second, the data were analyzed assuming that the most stable side chain binding conformations of the (AA)H^+(18C6) complexes were accessed in the experiments, that is, the ground-state conformation of the complex to Lys, and excited conformations of the complexes to His and Arg. In all cases, the experimental cross sections for reaction 3 are accurately reproduced using a loose PSL TS model.[66] Previous work has shown that this model provides the most accurate assessment of the kinetics shifts for CID processes for electrostatically bound ion−molecule complexes.[94−102] Good reproduction of the data is obtained over energy ranges exceeding 3.0 eV and cross-section magnitudes of at least a factor of 100. Table 2 lists values of the E_0 obtained without including the RRKM lifetime analysis. Comparison of these values with the E_0(PSL) values where lifetime effects are included shows that the kinetic shifts are the largest for the most strongly bound systems. The kinetic shifts observed for the (AA)H^+(18C6) complexes decrease in the order Gly > Ala > Lys > His > Arg. The same trend is found for the measured thresholds for loss of 18C6 from these complexes. Thus, the trend in the kinetic shift is consistent with expectations that the observed kinetic shift should directly correlate with the density of states of the activated complex at the threshold, which increases with energy.

For the (Gly)H^+(18C6) and (Ala)H^+(18C6) systems, the threshold determination is influenced by the competition among reactions 3 and 4. Therefore, the cross sections for reactions 3 and 4 were analyzed competitively using the model of eq 2 for these systems. The results of these analyses are provided in Table 2 and shown in Figure S4 of the Supporting Information. The (AA)H^+−18C6 BDEs obtained from competitive fits are larger than the values obtained from independent fits, and are in better agreement with the theoretical results for both the (Gly)H^+(18C6) and (Ala)-H^+(18C6) systems. The difference in the thresholds obtained from competitive and independent analyses generally allows the competitive shifts to be assessed. Determined in the usual way as the difference between the threshold determined for independent versus simultaneous analysis of the competitive CID thresholds, the competitive shifts for the (AA)H^+−18C6 BDEs are −0.35 and −0.21 eV for the complexes to Gly and Ala, respectively. The competitive shifts for the (18C6)H^+−AA BDEs are −0.19 and −0.20 eV for the Gly and Ala systems, respectively. The negative competitive shifts suggest that the competition sped up both pathways rather than retarding the less favorable dissociation pathway. This clearly makes no sense. In both systems, the independent fits to the H^+(AA) and H^+(18C6) product cross sections require larger n values (and therefore lead to lower threshold energies) in order to reproduce the slowly rising cross sections. In contrast, when competition is included, the slow rising behavior is shown to be a consequence of the competition and is properly handled by the model of eq 2, resulting in larger thresholds and lower n values. Thus, reliable thermochemistry can only be extracted from the CID thresholds for these systems when competitive effects are included.

The entropy of activation, $\Delta S^{\ddagger}$, is a measure of the looseness of the TS and the complexity of the system. It is determined from the molecular parameters used to model the EM and TS for dissociation as listed in Tables S1 and S2 of the Supporting Information. The $\Delta S^{\ddagger}$(PSL) values at 1000 K are listed in Table 2 and vary between 61 and 138 J/(K mol) across the these systems. The variation in the $\Delta S^{\ddagger}$ values is found to correlate directly with the size of the system and inversely with the strength of binding. For the (Gly)H^+(18C6) and (Ala)H^+(18C6) complexes, the entropy of activation is larger for the production of H^+(AA) as compared to H^+(18C6), indicating that the formation of H^+(AA) is entropically favorable as compared to the formation of H^+(18C6).

Conversion from 0 to 298 K. To allow comparison to commonly employed experimental conditions, we convert the 0 K BDEs determined here to 298 K bond enthalpies and free energies. The enthalpy and entropy conversions are calculated using standard formulas (assuming harmonic oscillator and rigid rotor models) and vibrational and rotational constants determined for the B3LYP/6-31G* optimized geometries, which are given in Tables S1 and S2 of the Supporting Information. Table S3 lists 0 and 298 K enthalpies, free energies, and enthalpic and entropic corrections for all systems experimentally determined. Enthalpic and entropic corrections are determined by ±10% variation in all vibrational frequencies,

dx.doi.org/10.1021/ja211021h | J. Am. Chem. Soc. 2012, 134, 5863−5875

and additionally by ±50% variation in the N−H···O frequencies associated with the noncovalent binding in these (AA)-H^+(18C6) complexes.

DISCUSSION

Comparison of Theory and Experiment. The measured and calculated (AA)H^+−18C6 BDEs for the complexes to Gly, Ala, Lys, His, and Arg and the (18C6)H^+−AA BDEs for the complexes to Gly and Ala at 0 K are summarized in Table 1. The agreement between theory and experiment is illustrated in Figure 5. Values for complexes to Lys, His, and Arg include the most stable conformers involving 18C6 binding to the protonated backbone as well as 18C6 binding to the protonated side chain. The measured (AA)H^+−18C6 BDEs exhibit excellent agreement with M06 theory assuming that the ground-state conformation are accessed in the experiments for all systems except the (His)H^+(18C6) complex. The mean absolute deviation (MAD) between M06 theory and experiment is 7.7 ± 10.9 kJ/mol when all five complexes are included, and decreases to 2.8 ± 2.1 kJ/mol when the (His)H^+(18C6) complex is not included. The agreement between B3LYP theory and the measured BDEs is less satisfactory. B3LYP theory systematically underestimates the measured (AA)H^+−18C6 BDEs by 39.2 ± 12.8 kJ/mol. In contrast, when the (His)H^+(18C6) complex is not included, the MAD becomes even worse, 43.4 ± 10.1 kJ/mol. However, the trend in the B3LYP calculated (AA)H^+−18C6 BDEs, Gly > Ala > Lys > His > Arg, parallels the measured values, whereas M06 theory reverses the relative affinities of His and Lys and finds Gly > Ala > His > Lys > Arg. This suggests that M06 theory may be overestimating the (His)H^+−18C6 BDE. If the most stable conformer involving 18C6 binding to the protonated side chain of His is accessed in the experiments rather than the calculated ground-state conformation, the MAD between M06 theory and experiment improves to 4.0 ± 3.2 kJ/mol, but degrades for B3LYP theory to 44.3 ± 9.0 kJ/mol. This suggests that an alternative explanation for the measured 18C6 affinities is that the side chain protonated species is accessed in measurable abundance in the ESI of these species. The average experimental uncertainty (AEU) for the measured (AA)H^+−18C6 BDEs is 7.2 ± 3.0 kJ/mol, is the same (or larger) than the MAD for M06 theory, but significantly smaller than that of B3LYP theory. Thus, M06 theory is clearly able to describe the hydrogen bonding interactions in these complexes much more accurately than B3LYP. The agreement is much better for the (Lys)H^+(18C6) complex when it is assumed that the ground-state side chain binding conformer is accessed in the experiments, and degrades significantly when it is assumed that an excited backbone binding conformer is accessed. In contrast, the agreement between theory and experiments for the (Arg)H^+(18C6) complex is excellent regardless of which structure is assumed to be accessed in the experiments.

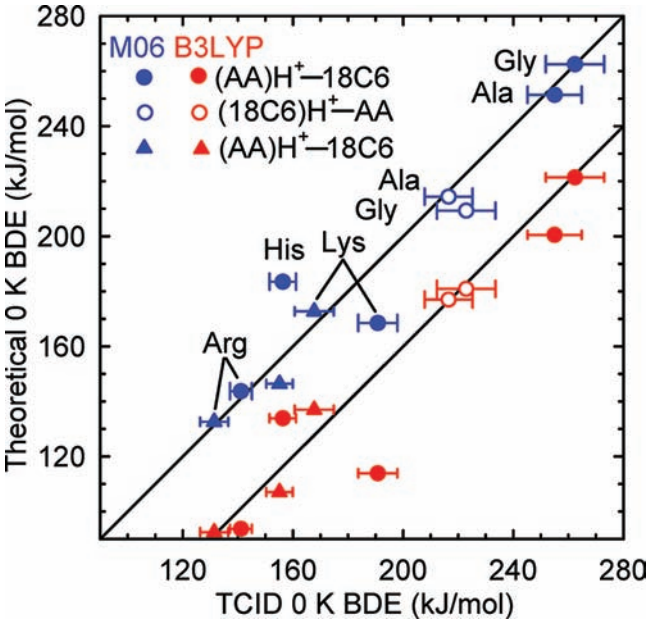

Figure 5. Theoretical versus experimental 0 K BDEs of complexes (AA)H^+(18C6). All values are taken from Tables 1. Values assuming that 18C6 binds to the protonated backbone amino group are plotted as circles, while values for 18C6 binding to the protonated side chain are plotted as triangles. Theoretical values plotted include ZPE and BSSE corrections.

The measured and calculated (18C6)H^+−AA BDEs of Gly and Ala at 0 K are also summarized in Table 1. Excellent agreement between M06 theory and the measured BDEs is also observed with a MAD of 7.9 ± 8.1 kJ/mol. Again, the agreement between B3LYP theory and the measured BDEs is less than satisfactory. B3LYP theory again systematically underestimates the measured (18C6)H^+−AA BDEs by 40.8 ± 1.8 kJ/mol. The AEU for the measured (18C6)H^+−AA BDEs is 9.6 ± 1.3 kJ/mol, is larger than the MAD for M06 theory, but also significantly smaller than that of B3LYP theory. Thus, M06 theory is clearly able to describe the hydrogen bonding interactions in these complexes much more accurately than B3LYP.

Trends in the 18C6 Binding Affinities. The measured (AA)H^+−18C6 BDEs determined here follow the order Gly > Ala > Lys > His > Arg. On the basis of the ground-state conformations computed for these five (AA)H^+(18C6) complexes (see Figure 3), 18C6 binds to the protonated backbone amino group in the complexes to Gly, Ala, Arg, and His, whereas binding to the protonated side chain substituent is preferred for the complex to Lys. In all cases, binding occurs via three nearly ideal N−H···O hydrogen bonds. The trends in the measured (AA)H^+−18C6 BDEs can be understood by examining steric interactions between 18C6 and the amino acid side chains. Gly and Ala bind most strongly because they possess the smallest side chain substituents, H and CH_3, and thus experience the least steric repulsion with 18C6. Lys exhibits the highest 18C6 affinity among the basic AAs examined here. Theoretical calculations indicate that binding to the protonated backbone amino group is favored over binding to the protonated side chain of His by 40.9 and 25.1 kJ/mol and of Arg by 13.9 and 5.8 kJ/mol (M06 and B3LYP theories, respectively). Thus, 18C6 binding to Lys side chains is clearly preferred over side chain binding to His and Arg. However, the present experimental results do not establish the relative preferences for side chain binding to His and Arg.

The analogous trend was also observed in our previous study of protonated peptidomimetic base−18C6 complexes.[41] The peptidomimetic bases that involve three N−H···O hydrogen bonds exhibit the highest binding affinities for 18C6. The Lys mimic, *n*-butylamine (NBA), exhibits a higher 18C6 binding affinity than the His mimics, imidazole (IMID) and 4-methylimidazole (4MeIMID), and the Arg mimic, 1-methyl-guanidine (MGD). The trend in the 18C6 binding affinity

dx.doi.org/10.1021/ja211021h | J. Am. Chem. Soc. 2012, 134, 5863−5875

between His and Arg is not readily predictable from the previous study, because the 18C6 binding affinity of the Arg mimic lies between that of the two His mimics, IMID and 4MeIMID. The 18C6 binding affinity of the Arg mimic, MGD, is 0.2 kJ/mol lower than that of the His mimic, IMID, but is 8.2 kJ/mol higher than the other His mimic, 4MeIMID.

Unfortunately the peptidomimetic bases employed in that study were not chosen in an entirely consistent fashion. 4MeIMID is a better mimic for the side chain of His than IMID, but rather than 1-methylguanidine, the best mimic for Arg would be 1-propylguanidine. The inverse correlation between the strength of binding in the $(B)H^+(18C6)$ complexes with the size/polarizability of the peptidomimetic base found suggests that 1-propylguanidine would bind less strongly than MGD by ~16 kJ/mol, or ~8 kJ/mol less strongly than 4MeIMID. This analysis suggests that His should bind 18C6 more strongly than Arg. While consistent with the trend measured here for His and Arg, theory suggests that the present results characterize the relative backbone affinities of these AAs.

Binding Sites of Amino Acid Side Chains. The measured 18C6 binding affinity for Lys is 11.4 kJ/mol higher than that of His, and 26.1 kJ/mol higher than that of Arg, suggesting that Lys is the preferred binding site for 18C6 complexation among the basic AAs in proteins or peptides. Much larger differences in the 18C6 binding preferences of the basic AAs are expected because the measured 18C6 binding affinities of His and Arg provide a measure of the binding to the protonated backbone amino group, which is calculated to be 40.9 and 13.9 kJ/mol (M06) more favorable than side chain binding, respectively. These results suggest that the Lys side chains are the preferred binding site for 18C6 complexation among the basic AAs in peptides and proteins. Similar results were also found in our previous study of protonated peptidomimetic bases with 18C6 complexes.[41] The 18C6 binding affinity of the Lys mimic, NBA, is 48.8 kJ/mol higher than that of the His mimic, IMID and 49.0 kJ/mol higher than that of the Arg mimic, MGD. The same general trend was also reported by Julian and Beauchamp[27] when a 1:1:1 mixture of NBA, guanidine (GD), and IMID was sprayed with 18C6. They found that the $(NBA)H^+(18C6)$ complex dominates the spectrum, and is the base peak (100% relative abundance), while the relative intensity of the $(GD)H^+(18C6)$ and $(IMID)H^+(18C6)$ complexes is 3.5% and 1%, respectively, suggesting that $H^+(NBA)$ binds 18C6 more strongly than $H^+(GD)$ and $H^+(IMID)$.

Gly and Ala exhibit higher 18C6 binding affinities than the other AAs examined here, suggesting that the N-terminal amino group could serve as an alternative binding site for 18C6 complexation. The methyl group of the Ala side chain increases the steric hindrance and constrains its complexation to 18C6. As a result, the 18C6 binding affinity of Ala is 7.4 kJ/mol lower than that of Gly. The X-ray study of Krestov and co-workers suggests that steric interactions with the N-terminal amino acid side chain could constrain its complexation with 18C6.[103] They found that the "depth of penetration" of the ammonium group into the 18C6 cavity for complexation exhibits a significant difference between diglycine and dialanine. The ammonium group in diglycine is much closer to the crown than that of dialanine during complexation. Steric interactions with the methyl side chain in proximity to the amino group in dialanine do not allow 18C6 to approach as closely and therefore bind as strongly. These and the present results suggest that the 18C6 binding affinity of the N-terminal amino group decreases as the size/polarizability of its side chain increases as a result of steric hindrance.

$(AA)H^+$−18C6 BDEs versus Polarizability of AA. In our previous study of the binding in protonated peptidomimetic base−18C6 complexes, $(B)H^+(18C6)$,[41] an inverse correlation between the 18C6 binding affinity and the polarizability of the base, B, was found. As can be seen in Figure 6a, an inverse correlation between the measured 18C6 binding affinities and the polarizability of neutral and protonated AAs is also found. Because the binding between 18C6 and the protonated AAs involves N−H···O hydrogen bonding interactions, the strength of binding should be controlled by ion-dipole and ion-induced dipole interactions. The polarizability of $H^+(Gly)$ is 5.5 Å^3, and increases to 7.2 Å^3 for $H^+(Ala)$, 13.5 Å^3 for Lys, 13.9 Å^3 for His, and 16.0 Å for Arg. The more polarizable AAs bind the proton

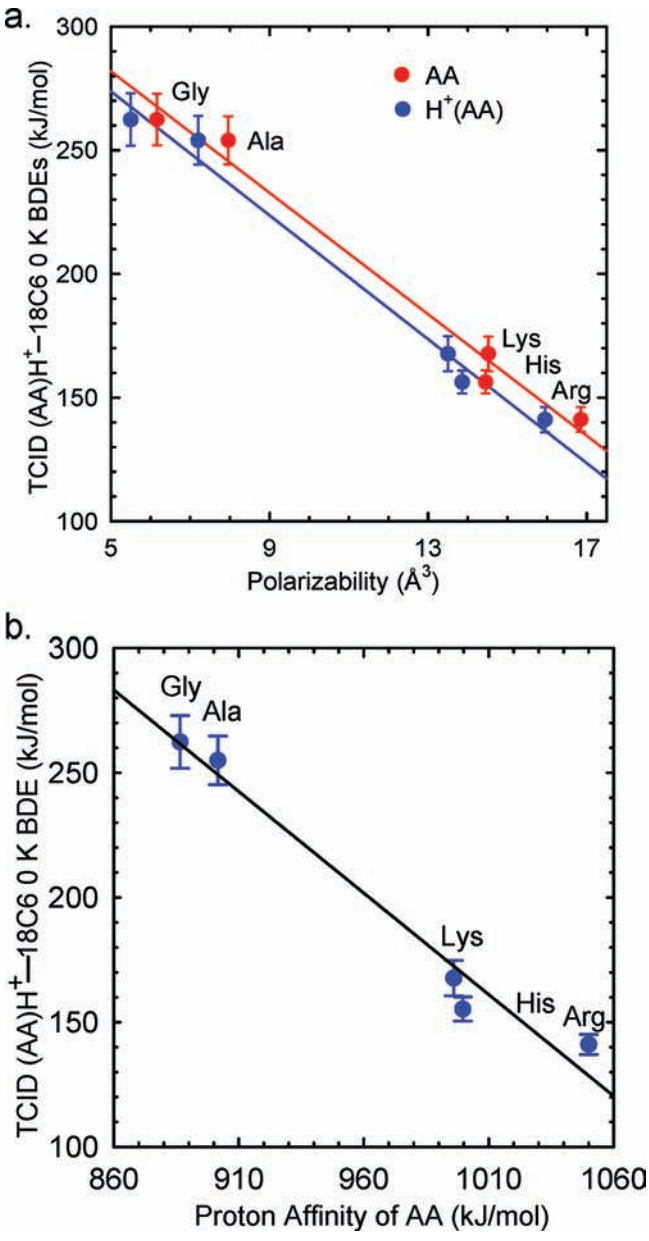

Figure 6. Measured $(AA)H^+$−18C6 BDEs at 0 K (kJ/mol) versus (a) PBE0/6-311+G(2d,2p) calculated polarizability of AA and $H^+(AA)$, and versus (b) the proton affinity of AA, where AA = Gly, Ala, Lys, His, and Arg. PAs taken from the NIST Webbook.[103−107].

dx.doi.org/10.1021/ja211021h | J. Am. Chem. Soc. 2012, 134, 5863−5875

more strongly and distribute the excess charge more evenly throughout the protonated base resulting in greater stabilization. The reduced charge on the protons of the amino group leads to weaker binding to 18C6. As a result, the 18C6 binding affinity decreases from 262.4 kJ/mol for Gly to 255.0 for Ala, to 167.7 kJ/mol for Lys, to 156.3 kJ/mol for His, and to 141.1 kJ/mol for Arg. A parallel correlation between the measured BDEs and the polarizability of the neutral AAs is also obviously found, as the proton merely decreases the polarizability slightly.

(AA)H$^+$−18C6 BDEs versus PA of AA. The measured 18C6 binding affinity was also shown to exhibit an inverse linear correlation with the PA of the peptidomimetic base as a result of the shorter N−H bonds and the decreased charge retained on the amino protons. An inverse correlation between the measured 18C6 binding affinity and the PA of the AAs is also observed in the systems examined here, as shown in Figure 6b. The PA of Gly is 886.5 kJ/mol, and increases to 901.6 kJ/mol for Ala, 996.0 kJ/mol for Lys, 999.6 kJ/mol for His,[104] and 1051.0 kJ/mol for Arg.[105−107] Accordingly, the measured (AA)H$^+$−18C6 BDEs decrease from 262.4 kJ/mol for Gly, to 255.0 kJ/mol for Ala, 167.7 kJ/mol for Lys, 156.3 kJ/mol for His, and 141.1 kJ/mol for Arg. This inverse correlation is understood by the fact that the AA with a higher PA binds the proton tighter and leads to weaker hydrogen-bonding interactions with 18C6, resulting in lower dissociation thresholds. That is, the binding is strongest when the PAs of the AA and 18C6 are similar such that the proton is more equally shared.

Competitive Reaction Pathways. In the (Gly)H$^+$(18C6) and (Ala)H$^+$(18C6) complexes, H$^+$(AA) was observed in competition with the formation of H$^+$(18C6). The cross sections for these products are large enough to significantly influence the kinetics of dissociation for the primary CID pathway. Therefore, a loose PSL TS was used to analyze the H$^+$(AA) and H$^+$(18C6) product cross sections competitively. The results of the competitive analyses of the cross sections of the H$^+$(AA) and H$^+$(18C6) products exhibit excellent agreement with M06 theory indicating that the loose PSL TS model accurately describes the binding in theses systems.

Entropy Effects. The NIST Chemistry WebBook suggests that the PA of 18C6 is 967.0 kJ/mol, higher than the PAs of both Gly and Ala, 886.5 and 901.6 kJ/mol, respectively. Therefore, H$^+$(18C6) was observed as a major and the lowest energy CID product in the (Gly)H$^+$(18C6) and (Ala)H$^+$(18C6) complexes. Interestingly, H$^+$(AA) is also observed as a competitive CID product. This phenomenon can be understood by considering the change in entropy associated with the dissociation pathways. Entropy effects on CID results have been addressed by McLuckey and Cooks.[91,108−110] Wesdemiotis reported that entropy changes involved in the fragmentation of heterodimers play a critical role in determining the preferred dissociation pathway.[109] For the (Gly)H$^+$(18C6) and (Ala)H$^+$(18C6) systems, the reaction pathway that involves formation of H$^+$(AA) exhibits a greater increase in entropy than the H$^+$(18C6) pathway. In the ground-state structure of H$^+$(18C6), the proton is bound to one oxygen atom and is stabilized by a hydrogen bonding interaction with another oxygen atom, which results in more constrained rotational and vibration degrees of freedom in the protonated complex of 18C6. Therefore, the relatively favorable entropy change as compared to the formation of H$^+$(18C6) facilitates the formation of H$^+$(AA), making the formation of H$^+$(AA) as a CID product feasible even though the AA exhibits a much lower PA than 18C6. For example, in the (Gly)H$^+$(18C6) and (Ala)H$^+$(18C6) systems, elimination of H$^+$(AA) leads to a large gain in rotational and vibrational degrees of freedom of 18C6, resulting in a substantial increase in entropy for this competitive reaction pathway. In contrast, the formation of H$^+$(18C6) results in entropic loss as compared to the H$^+$(AA) competitive dissociation pathway. Therefore, the kinetics of dissociation are slowed down, resulting in a more significant kinetic shift as compared to the H$^+$(AA) pathway. As a result, despite the fact that the PAs of Gly and Ala are 80.5 and 65.4 kJ/mol lower than that of 18C6, respectively, the dissociation pathway that forms H$^+$(AA) is still observed and dominates at elevated energies.

The magnitudes of the CID product cross sections for H$^+$(AA) and H$^+$(18C6) are the result of competition between enthalpy and entropy: entropy favors the formation of H$^+$(AA), while enthalpy favors the formation of the species that exhibits the higher PA. In the Lys, His, and Arg containing systems, the AA exhibits a higher PA than 18C6. Therefore, enthalpy favors the formation of H$^+$(AA). The relatively favorable entropy change as compared to the formation of H$^+$(18C6) also favors the formation of H$^+$(AA). As a result, H$^+$(AA) and its fragments were observed as the only CID products. In contrast, in the complexes involving Gly and Ala, the PA of 18C6 exceeds that of the AA. Therefore, enthalpy favors the formation of H$^+$(18C6). As a result, H$^+$(18C6) was observed as the lowest energy CID product. However, because entropy favors the formation of H$^+$(AA), it is observed as a competitive CID product.

■ CONCLUSIONS

The kinetic energy dependence for CID of five (AA)H$^+$(18C6) complexes, where AA = Gly, Ala, Lys, His, and Arg, with Xe is examined by guided ion beam tandem mass spectrometry techniques. Loss of the intact 18C6 ligand is observed for all five complexes, and corresponds to the most favorable process for the complexes to Lys, His, and Arg. For the complexes to Gly and Ala, loss of the intact AA is observed in competition with loss of 18C6 and corresponds to the lowest-energy pathway for these complexes. Thresholds for these CID processes are determined after consideration of the effects of the kinetic and internal energy distributions of the reactants, multiple collisions with Xe, and the lifetimes for unimolecular dissociation. The ground-state structures and theoretical estimates for the CID thresholds are determined from density functional theory calculations performed at the B3LYP/6-311+G(2d,2p)//B3LYP/6-31G* and M06/6-311+G(2d,2p)//B3LYP/6-31G* levels of theory. Excellent agreement between M06 theoretically calculated and experimentally determined BDEs was found for all systems except (His)H$^+$(18C6) where either theory overestimates the strength of binding or excited conformers are accessed in these experiments. In contrast, B3LYP theory systematically underestimates the strength of binding in all of these systems.

The 18C6 binding affinities determined here combined with structural information obtained from theoretical calculations provides useful insight into the processes that occur in the molecular recognition of AAs by 18C6 and implications for binding to peptides and proteins. Among the basic AAs, Lys exhibits the highest binding affinity for 18C6, suggesting that the side chains of Lys residues are the preferred binding sites for 18C6. Gly and Ala exhibit greater 18C6 binding affinities than Lys, suggesting that the N-terminal amino group could

also serve as a favorable binding site for 18C6. The 18C6 binding affinity exhibits an inverse correlation with the polarizability and PA of the AA. Thus, the ability of the N-terminal amino group to serve as a binding site for 18C6 requires that it be protonated and accessible in the peptide or protein. Binding of 18C6 to the N-terminal amino group will be most effective for Gly and becomes increasingly less favorable as the size and proton affinity of the AA increases.

■ ASSOCIATED CONTENT

Supporting Information

Complete citation for ref 52. Tables of vibrational frequencies, average vibrational energies at 298 K, rotational constants, and enthalpies and free energies of H^+(AA) binding to 18C6, and H^+(18C6) binding to AA at 298 K. Figures showing cross sections for CID and thermochemical analyses of zero-pressure extrapolated CID cross sections for the (AA)H^+(18C6) complexes. Ground-state and stable low-energy structures of the neutral and protonated AAs and 18C6 and proton bound complexes composed of these species, (AA)H^+(18C6). This material is available free of charge via the Internet at http://pubs.acs.org.

■ AUTHOR INFORMATION

Corresponding Author

mrodgers@chem.wayne.edu

Notes

The authors declare no competing financial interest.

■ ACKNOWLEDGMENTS

This work is supported by the National Science Foundation, Grant CHE-0911191. The authors also thank Wayne State University C&IT for computer time and support.

■ REFERENCES

(1) Clackson, T.; Ultsch, M. H.; Wells, J. A.; Vos, A. M. D. *J. Mol. Biol.* **1998**, *277*, 1111.
(2) Wells, J. A. *Proc. Natl. Acad. Sci. U.S.A.* **1996**, *93*, 1.
(3) Bogan, A. A.; Thorn, K. S. *J. Mol. Biol.* **1998**, *280*, 1.
(4) Clackson, T.; Wells, J. A. *Science* **1995**, *267*, 383.
(5) Matthews, B. W. *Annu. Rev. Phys. Chem.* **1976**, *27*, 493.
(6) Dyson, H. J.; Wright, P. E. *Chem. Rev.* **2004**, *104*, 3607.
(7) Palmer, A. G. *Chem. Rev.* **2004**, *104*, 3623.
(8) Mendoza, V. L.; Vachet, R. W. *Mass Spectrom. Rev.* **2009**, *28*, 785.
(9) Wales, T. E.; Engen, J. R. *Mass Spectrom. Rev.* **2006**, *25*, 158.
(10) Smith, D. L.; Deng, Y.; Zhang, Z. *J. Mass Spectrom.* **1997**, *32*, 135.
(11) Engen, J. R.; Smith, D. L. *Anal. Chem.* **2001**, *73*, 256A.
(12) Kaltashov, I. A.; Eyles, S. J. *Mass Spectrom. Rev.* **2002**, *21*, 37.
(13) Kaltashov, I. A.; Eyles, S. J. *Mass Spectrom. Rev.* **2002**, *37*, 557.
(14) Hoofnagle, A. N.; Resing, K. A.; Ahn, N. G. *Annu. Rev. Biophys. Biomol. Struct.* **2003**, *32*, 1.
(15) Eyles, S. J.; Kaltashov, I. A. *Methods* **2004**, *34*, 88.
(16) Garcia, R. A.; Pantazatos, D.; Villarreal, F. J. *Assay Drug Dev. Technol.* **2004**, *2*, 81.
(17) Sinz, A. *J. Mass Spectrom.* **2003**, *38*, 1225.
(18) Sinz, A. *Mass Spectrom. Rev.* **2006**, *25*, 663.
(19) Brunner, J. *Annu. Rev. Biochem.* **1993**, *62*, 483.
(20) Kluger, R.; Alagic, A. *Bioorg. Chem.* **2004**, *32*, 451.
(21) Melcher, K. *Curr. Protein Pept. Sci.* **2004**, *5*, 287.
(22) Kodadek, T.; Duroux-Richard, I.; Bonnafous, J. C. *Trends Pharmacol. Sci.* **2005**, *26*, 210.
(23) Back, J. W.; de Jong, L.; Muijsers, A. O.; de Koster, C. G. *J. Mol. Biol.* **2003**, *331*, 303.
(24) Friedhoff, P. *Anal. Bioanal. Chem.* **2005**, *381*, 78.
(25) Trakselis, M. A.; Alley, S. C.; Ishmael, F. T. *Bioconjugate Chem.* **2005**, *16*, 741.
(26) Petrotchenko, E. V.; Pedersen, L. C.; Borchers, C. H.; Tomer, K. B.; Negishi, M. *FEBS Lett.* **2001**, *490*, 39.
(27) Julian, R. R.; Beauchamp, J. L. *Int. J. Mass Spectrom.* **2001**, *210/211*, 613.
(28) Julian, R. R.; Beauchamp, J. L. *J. Am. Soc. Mass Spectrom.* **2002**, *13*, 493.
(29) Julian, R. R.; Beauchamp, J. L. *J. Am. Soc. Mass Spectrom.* **2004**, *15*, 616.
(30) Julian, R. R.; Akin, M.; May, J. A.; Stoltz, B. M.; Beauchamp, J. L. *Int. J. Mass Spectrom.* **2002**, *220*, 87.
(31) Julian, R. R.; May, J. A.; Stoltz, B. M.; Beauchamp, J. L. *Int. J. Mass Spectrom.* **2003**, *228*, 851.
(32) Ly, T.; Julian, R. R. *J. Am. Soc. Mass Spectrom.* **2006**, *17*, 1209.
(33) Ly, T.; Julian, R. R. *J. Am. Soc. Mass Spectrom.* **2008**, *19*, 1663.
(34) Liu, Z.; Cheng, S.; Gallie, D. R.; Julian, R. R. *Anal. Chem.* **2008**, *80*, 3846.
(35) Ly, T.; Liu, Z.; Pujanauski, B. G.; Sarpong, R.; Julian, R. R. *Anal. Chem.* **2008**, *80*, 5059.
(36) Yeh, G. K.; Sun, Q.; Meneses, C.; Julian, R. R. *J. Am. Soc. Mass Spectrom.* **2009**, *20*, 385.
(37) Weimann, D. P.; Winkler, H. D. F.; Falenski, J. A.; Koksch, B.; Schalley, C. A. *Nat. Chem.* **2009**, *1*, 573.
(38) Pagel, K.; Hyung, S. J.; Ruotolo, B. T.; Robinson. *Anal. Chem.* **2010**, *82*, 5363.
(39) Wilson, J. J.; Kirkovits, G. J.; Sessler, J. L.; Brodbelt, J. S. *J. Am. Soc. Mass Spectrom.* **2008**, *19*, 257.
(40) Oshima, T.; Suetsugu, A.; Baba, Y. *Anal. Chim. Acta* **2010**, *674*, 211.
(41) Chen, Y; Rodgers, M. T. *J. Am. Chem. Soc.* **2012**, *134*, 2313.
(42) Rodgers, M. T. *J. Phys. Chem. A* **2001**, *105*, 2374.
(43) Moison, R. M.; Armentrout, P. B. *J. Am. Soc. Mass Spectrom.* **2007**, *18*, 1124.
(44) Shaffer, S. A.; Prior, D. C.; Anderson, G. A.; Udseth, H. R.; Smith, R. D. *Anal. Chem.* **1998**, *70*, 4111.
(45) Shaffer, S. A.; Tolmachev, A.; Prior, D. C.; Anderson, G. A.; Udseth, H. R.; Smith, R. D. *Anal. Chem.* **1999**, *71*, 2957.
(46) Teloy, E.; Gerlich, D. *Chem. Phys.* **1974**, *4*, 417.
(47) Aristov, N.; Armentrout, P. B. *J. Phys. Chem.* **1986**, *90*, 5135.
(48) Hales, D. A.; Armentrout, P. B. *J. Cluster Sci.* **1990**, *1*, 127.
(49) Ervin, K. M.; Armentrout, P. B. *J. Chem. Phys.* **1985**, *83*, 166.
(50) Dalleska, N. F.; Honma, K.; Sunderlin, L. S.; Armentrout, P. B. *J. Am. Chem. Soc.* **1994**, *116*, 3519.
(51) *HyperChem Computational Chemistry Software Package*, Version 5.0; Hypercube, Inc.: Gainsville, FL, 1997.
(52) Frisch, M. J.; et al. *Gaussian 09*, Revision C.01; Gaussian, Inc.: Wallingford, CT, 2009. See Supporting Information for full reference.
(53) Becke, A. D. *J. Chem. Phys.* **1993**, *98*, 5648.
(54) Lee, C.; Yang, W.; Parr, R. G. *Phys. Rev. B* **1988**, *37*, 785.
(55) Foresman, J. B.; Frisch, Æ. *Exploring Chemistry with Electronic Structure Methods*, 2nd ed.; Gaussian: Pittsburgh, PA, 1996; p 64.
(56) Boys, S. F.; Bernardi, R. *Mol. Phys.* **1979**, *19*, 553.
(57) van Duijneveldt, F. B.; van Duijneveldt-van de Rijdt, J. G. C. M.; van Lenthe, J. H. *Chem. Rev.* **1994**, *94*, 1873.
(58) Adamo, C.; Barone, V. *J. Chem. Phys.* **1999**, *110*, 6158.
(59) Smith, S. M; Markevitch, A. N.; Romanov, D. A.; Li, X.; Levis, R. J.; Schlegel, H. B. *J. Phys. Chem. A* **2004**, *108*, 11063.
(60) Muntean, F.; Armentrout, P. B. *J. Chem. Phys.* **2001**, *115*, 1213.
(61) Beyer, T. S.; Swinehart, D. F. *Commun. ACM* **1979**, *16*, 379.
(62) Stein, S. E.; Rabinovitch, B. S. *J. Chem. Phys.* **1973**, *58*, 2438.
(63) Stein, S. E.; Rabinovitch, B. S. *Chem. Phys. Lett.* **1977**, *49*, 183.
(64) Pople, J. A.; Schlegel, H. B.; Raghavachari, K.; DeFrees, D. J.; Binkley, J. F.; Frisch, M. J.; Whitesides, R. F.; Hout, R. F.; Hehre, W. J. *Int. J. Quantum Chem., Symp.* **1981**, *15*, 269.
(65) DeFrees, D. J.; McLean, A. D. *J. Chem. Phys.* **1985**, *82*, 333.
(66) Rodgers, M. T.; Ervin, K. M.; Armentrout, P. B. *J. Chem. Phys.* **1997**, *106*, 4499.

(67) Khan, F. A.; Clemmer, D. E.; Schultz, R. H.; Armentrout, P. B. *J. Phys. Chem.* **1993**, *97*, 7978.
(68) Chesnavich, W. J.; Bowers, M. T. *J. Phys. Chem.* **1979**, *83*, 900.
(69) Yang, Z.; Rodgers, M. T. *Phys. Chem. Chem. Phys.* **2004**, *6*, 2749.
(70) Yang, Z.; Rodgers, M. T. *J. Am. Chem. Soc.* **2004**, *126*, 16217.
(71) Rannulu, N. S.; Rodgers, M. T. *Phys. Chem. Chem. Phys.* **2005**, *7*, 1014.
(72) Ruan, C.; Rodgers, M. T. *J. Am. Chem. Soc.* **2004**, *126*, 14600.
(73) Ruan, C.; Rodgers, M. T. *J. Am. Chem. Soc.* **2009**, *131*, 10918.
(74) Ruan, C.; Yang, Z.; Rodgers, M. T. *Phys. Chem. Chem. Phys.* **2007**, *9*, 5902.
(75) Chinthaka, S. D. M.; Chu, Y.; Rannulu, N. S.; Rodgers, M. T. *J. Phys. Chem. A* **2007**, *110*, 1426.
(76) Chinthaka, S. D. M.; Rodgers, M. T. *J. Phys. Chem. A* **2006**, *111*, 8152.
(77) Rannulu, N. S.; Rodgers, M. T. *Phys. Chem. Chem. Phys.* **2005**, *7*, 1014.
(78) Rannulu, N. S.; Amunugama, R.; Yang, Z.; Rodgers, M. T. *J. Phys. Chem. A* **2004**, *108*, 6385.
(79) Amunugama, R.; Rodgers, M. T. *Int. J. Mass. Spectrom.* **2003**, *227*, 1.
(80) Amunugama, R.; Rodgers, M. T. *J. Phys. Chem. A* **2002**, *106*, 9718.
(81) Dalleska, N. F.; Honma, K.; Armentrout, P. B. *J. Am. Chem. Soc.* **1993**, *115*, 12125.
(82) Armentrout, P. B.; Simons, J. *J. Am. Chem. Soc.* **1992**, *114*, 8627.
(83) Rodgers, M. T.; Armentrout, P. B. *Mass Spectrom. Rev.* **2000**, *19*, 215.
(84) Yalcin, T.; Harrison, A. G. *J. Mass Spectrom.* **1996**, *31*, 1237.
(85) Iris Shek, P. Y.; Zhao, J.; Ke, Y.; Siu, K. W. M.; Hopkinson, A. C. *J. Phys. Chem. A* **2006**, *110*, 8282.
(86) Zhang, K.; Zimmerman, D. M.; Chung-Phillips, A.; Cassady, C. J. *J. Am. Chem. Soc.* **1993**, *115*, 10812.
(87) Armentrout, P. B.; Heaton, A. L.; Ye, S. J. *J. Phys. Chem. A* **2011**, *115*, 11144.
(88) Lemoff, A. S.; Bush, M. F.; O'Brien, J. T.; Williams, E. R. *J. Phys. Chem. A* **2006**, *110*, 8433.
(89) Dunbar, R. C.; Hopkinson, A. C.; Oomens, J.; Siu, C. K.; Siu, K. W. M.; Steill, J. D.; Verkerk, U. H.; Zhao, J. *J. Phys. Chem. B* **2009**, *113*, 10403.
(90) Kovacevic, B.; Rozman, M.; Klasinc, L.; Srzic, D.; Maksic, Z. B.; Yanez, M. *J. Phys. Chem. A* **2005**, *109*, 8329.
(91) Bliznyuk, A. A.; Schaefer, H. F. III; Amster, I. J. *J. Am. Chem. Soc.* **1993**, *115*, 5149.
(92) Ling, S.; Yu, W.; Huang, Z.; Lin, Z.; Haranczyk, M.; Gutowski, M. *J. Phys. Chem. A* **2006**, *110*, 12282.
(93) Forbes, M. W.; Bush, M. F.; Polfer, N. C.; Oomens, J.; Dunbar, R. C.; Williams, E. R.; Jockusch, R. A. *J. Phys. Chem. A* **2007**, *111*, 11759.
(94) Rodgers, M. T.; Armentrout, P. B. *J. Phys. Chem. A* **1997**, *101*, 1238.
(95) Rodgers, M. T.; Armentrout, P. B. *J. Phys. Chem. A* **1997**, *101*, 2614.
(96) Rodgers, M. T.; Armentrout, P. B. *Int. J. Mass Spectrom.* **1999**, *185/186/187*, 359.
(97) Rodgers, M. T.; Armentrout, P. B. *J. Phys. Chem. A* **1999**, *103*, 4955.
(98) Armentrout, P. B.; Rodgers, M. T. *J. Phys. Chem. A* **1999**, *104*, 2238.
(99) Amunugama, R.; Rodgers, M. T. *Int. J. Mass Spectrom.* **2000**, *195/196*, 439.
(100) Rodgers, M. T.; Armentrout, P. B. *J. Am. Chem. Soc.* **2000**, *122*, 8548.
(101) Rodgers, M. T.; Armentrout, P. B. *J. Chem. Phys.* **1998**, *109*, 1787.
(102) Rodgers, M. T. *J. Phys. Chem. A* **2001**, *105*, 8145.
(103) Kulikov, O. V.; Krestov, G. A. *Pure Appl. Chem.* **1995**, *67*, 1103.
(104) Bouchoux, G.; Bussson, D. A.; Colas, C.; Sablier, M. *Eur. J. Mass Spectrom.* **2004**, *10*, 977.
(105) Hunter, E. P.; Lias, S. G. *J. Phys. Chem. Ref. Data* **1998**, *27*, 413.
(106) Bouchoux, G.; Salpin, J. Y. *Eur. J. Mass Spectrom.* **2003**, *9*, 391.
(107) Meot-Ner, M.; Hunter, E.; Field, F. H. *J. Am. Chem. Soc.* **1979**, *101*, 686.
(108) McLuckey, S. A.; Cooks, R. G.; Fulford, J. E. *Int. J. Mass Spectrom. Ion Phys.* **1983**, *52*, 165.
(109) Cerda, B. A.; Wesdemiotis, C. *J. Am. Chem. Soc.* **1996**, *118*, 11884.
(110) Cheng, X.; Wu, Z.; Fenselau, C. *J. Am. Chem. Soc.* **1993**, *115*, 4844.